doi:10.1093/brain/awv385 BRAIN 2016: 139; 937–952 | 937

BRAIN
A JOURNAL OF NEUROLOGY

# Improved proteostasis in the secretory pathway rescues Alzheimer's disease in the mouse

**Yajing Peng,[1] Mi Jin Kim,[2] Rikki Hullinger,[1,3] Kenneth J. O'Riordan,[4,*] Corinna Burger,[3,4] Mariana Pehar[2] and Luigi Puglielli[1,3,5,6,7]**

See Duran-Aniotz *et al.* (doi:10.1093/brain/awv401) for a scientific commentary on this article.

The aberrant accumulation of toxic protein aggregates is a key feature of many neurodegenerative diseases, including Huntington's disease, amyotrophic lateral sclerosis and Alzheimer's disease. As such, improving normal proteostatic mechanisms is an active target for biomedical research. Although they share common pathological features, protein aggregates form in different subcellular locations. Nε-lysine acetylation in the lumen of the endoplasmic reticulum has recently emerged as a new mechanism to regulate the induction of autophagy. The endoplasmic reticulum acetylation machinery includes AT-1/SLC33A1, a membrane transporter that translocates acetyl-CoA from the cytosol into the endoplasmic reticulum lumen, and ATase1 and ATase2, two acetyltransferases that acetylate endoplasmic reticulum cargo proteins. Here, we used a mutant form of α-synuclein to show that inhibition of the endoplasmic reticulum acetylation machinery specifically improves autophagy-mediated disposal of toxic protein aggregates that form within the secretory pathway, but not those that form in the cytosol. Consequently, haploinsufficiency of AT-1/SLC33A1 in the mouse rescued Alzheimer's disease, but not Huntington's disease or amyotrophic lateral sclerosis. In fact, intracellular toxic protein aggregates in Alzheimer's disease form within the secretory pathway while in Huntington's disease and amyotrophic lateral sclerosis they form in different cellular compartments. Furthermore, biochemical inhibition of ATase1 and ATase2 was also able to rescue the Alzheimer's disease phenotype in a mouse model of the disease. Specifically, we observed reduced levels of soluble amyloid-β aggregates, reduced amyloid-β pathology, reduced phosphorylation of tau, improved synaptic plasticity, and increased lifespan of the animals. In conclusion, our results indicate that Nε-lysine acetylation in the endoplasmic reticulum lumen regulates normal proteostasis of the secretory pathway; they also support therapies targeting endoplasmic reticulum acetyltransferases, ATase1 and ATase2, for a subset of chronic degenerative diseases.

1 Department of Medicine, University of Wisconsin-Madison, Madison, WI, USA
2 Department of Cell and Molecular Pharmacology and Experimental Therapeutics, Medical University of South Carolina, Charleston, SC, USA
3 Neuroscience Training Program, University of Wisconsin-Madison, Madison, WI, USA
4 Department of Neurology, University of Wisconsin-Madison, Madison, WI, USA
5 Geriatric Research Education Clinical Center, VA Medical Center, Madison, WI, USA
6 Department of Neuroscience, University of Wisconsin-Madison, Madison, WI, USA
7 Wisconsin Alzheimer's Disease Research Center, University of Wisconsin-Madison, Madison, WI, USA

*Present address: Department of Pharmacology and Therapeutics, Trinity College, Dublin 2, Ireland

Correspondence to: Luigi Puglielli,
Department of Medicine,
University of Wisconsin-Madison,
Madison, WI,
USA
E-mail: lp1@medicine.wisc.edu

Received July 14, 2015. Revised September 29, 2015. Accepted November 4, 2015. Advance Access publication January 19, 2016

Correspondence may also be addressed to: Mariana Pehar, Department of Cell and Molecular Pharmacology and Experimental Therapeutics, Medical University of South Carolina, Charleston, SC, USA. E-mail: pehar@musc.edu

**Keywords:** AT-1/SLC33A1; ATase; lysine acetylation; proteostasis; Alzheimer's disease; autophagy

**Abbreviations:** AT-1 = acetyl CoA transporter 1; ATase1 = acetyltransferase 1; ATase2 = acetyltransferase 2; Atg = autophagy protein; ER = endoplasmic reticulum; MEF = mouse embryo fibroblast

# Introduction

Integral membrane proteins and secretory proteins are typically synthesized at the surface of the endoplasmic reticulum (ER) where they also enter the secretory pathway (Wickner and Schekman, 2005). Proteins that are not required to enter the secretory pathway are instead synthesized in the cytosol. Independently from where they are synthesized, all new polypeptides are selected based on their ability to fold. The quality control machinery that selects correctly folded and unfolded/misfolded polypeptides is tightly linked to the degrading machinery so that unfolded/misfolded polypeptides can be disposed of, thus ensuring fidelity of the protein code (Trombetta and Parodi, 2003).

Autophagy is an essential component of the degrading machinery. It helps dispose of large toxic protein aggregates that form within the secretory pathway as well as in the cytosol. Malfunction of autophagy contributes to the progression of many chronic diseases, including neurodegeneration, cancer, nephropathies, immune and cardiovascular diseases (reviewed in Nixon, 2013; Frake *et al.*, 2015; Levine *et al.*, 2015). In addition, many chronic degenerative diseases are characterized by the aberrant accumulation of toxic protein aggregates. As such, improving normal proteostatic mechanisms is an active target for biomedical research (Mizushima *et al.*, 2008; Levine *et al.*, 2015).

Compelling data indicate that both hypoactive and hyperactive autophagy can be detrimental for the organism (reviewed in Frake *et al.*, 2015; Levine *et al.*, 2015). The same data also indicate that increased levels of autophagy, which are pathogenic in wild-type mice in the absence of toxic protein aggregates, can be beneficial in mouse models of diseases characterized by increased accumulation of toxic protein aggregates (van Dellen *et al.*, 2000; Pickford *et al.*, 2008; Hetz *et al.*, 2009; Madeo *et al.*, 2009; Bhuiyan *et al.*, 2013). As toxic protein aggregates can form in different locations (i.e. within the secretory pathway or in the cytosol), it is likely that different signals are used to trigger autophagy.

Many integral membrane proteins and secretory proteins that enter the secretory pathway undergo transient Nε-lysine acetylation within the lumen of the ER (Choudhary *et al.*, 2009; Pehar *et al.*, 2012*a*). The acetylation of ER cargo proteins requires active transport of acetyl-CoA from the cytosol into the ER lumen by AT-1/SLC33A1, and the acetyltransferase activity of two ER membrane proteins, ATase1 and ATase2 (reviewed in Pehar and Puglielli, 2013). ATase1 (encoded by *NAT8B*) and ATase2 (encoded by *NAT8*) were recently found to associate with the oligosaccharyl transferase complex and acetylate correctly folded polypeptides (Ding *et al.*, 2014). Studies conducted with two substrates of the ATases, BACE1 and CD133 (encoded by *PROM1*), suggest that Nε-lysine acetylation might be part of normal quality control to select correctly folded polypeptides (Costantini *et al.*, 2007; Ko and Puglielli, 2009; Ding *et al.*, 2014; Mak *et al.*, 2014). Importantly, the promoter of AT-1 has an X-box binding protein 1 (XBP1) binding element and, as a result, the expression of AT-1 is activated by XBP1 during the unfolded protein response to partially repress the induction of autophagy (Pehar *et al.*, 2012*b*). Downregulation or inactivation of AT-1 in isolated cells or in the animal leads to increased autophagy (Jonas *et al.*, 2010; Pehar *et al.*, 2012*b*; Peng *et al.*, 2014). Therefore, the above studies suggest that the ER acetylation machinery might participate in the regulation of quality control as well as ER-associated degradation type II/autophagy.

Data from yeast, *Drosophila melanogaster*, *Caenorhabditis elegans*, and mammals indicate that Nε-lysine acetylation can serve as a master regulator of the autophagic response to a large variety of insults (reviewed in Madeo *et al.*, 2009, 2010). In addition to possible global epigenetic control of autophagy proteins induced by changes in acetyl-CoA levels (Eisenberg *et al.*, 2014; Marino *et al.*, 2014), acetylation and deacetylation of selective members of the autophagy machinery, such as ATG9A, ATG5, ATG7, Atg8/GABARAP) and ATG12, can also regulate the induction and/or progression of autophagy. More specifically, Nε-lysine acetylation inhibits while Nε-lysine deacetylation stimulates autophagy (Lee *et al.*, 2008; Lee and Finkel, 2009; Pehar *et al.*, 2012*b*). Improved autophagic functions that result from reduced acetylation and/or increased deacetylation have been associated with more efficient protein and organelle homeostasis, cytoprotection, lifespan extension, and rescue of proteotoxic phenotypes (reviewed in Madeo *et al.*, 2015).

Here, we report that inhibition of the ER acetylation machinery stimulates the disposal of toxic protein aggregates that form within the secretory pathway but not those that form in other compartments. Consistently, genetic or biochemical inhibition of the acetylation machinery in the mouse rescued the Alzheimer's disease phenotype, but not the Huntington's disease or the amyotrophic lateral sclerosis phenotypes.

# Materials and methods

The following experimental approaches have been described in detail previously: lactate dehydrogenase (LDH) activity in the conditioned media (Costantini *et al.*, 2005); electrophysiology of hippocampal brain slices (Pehar *et al.*, 2010); and enzyme-linked immunosorbent assay (ELISA) of soluble amyloid-β (Costantini *et al.*, 2006; Pehar *et al.*, 2010).

## Cells and animals

Mouse embryonic fibroblasts (MEFs) from wild-type and AT-$1^{S113R/+}$ mice were described previosuly (Peng *et al.*, 2014). MEFs, Chinese Hamster Ovary (CHO), and human neuroglioma (H4) cells were maintained in Dulbecco's modified Eagle medium supplemented with 10% foetal bovine serum (FBS) and 1% penicillin/streptomycin/glutamine solution (Mediatech). CHO cell transfection was performed using Lipofectamine™ 2000 (Invitrogen/Life Technologies). MEFs were transfected with Amaxa™ Basic Nucleofector™ Kit for Primary Mammalian Fibroblasts (Lonza). Cells were harvested 48 h later for western blot or immunostaining.

AT-$1^{S113R/+}$ and $APP_{695/swe}$ mice were described previously (Pehar *et al.*, 2010; Peng *et al.*, 2014). $mHtt^{Q160}$ (also known as R6/2) and $hSOD1^{G93A}$ mice were from The Jackson Laboratory. The rodent diet with Compound 9 was manufactured by Bio-Serv. The same diet without compound served as the control diet.

All animal experiments were carried out in accordance with the NIH Guide for the Care and Use of Laboratory Animals and were approved by the Institutional Animal Care and Use Committee of the University of Wisconsin-Madison and the Madison Veterans Administration Hospital.

## Protein extraction and western blotting

Protein extracts (Peng *et al.*, 2014) and extracellular enriched proteins (Lesne *et al.*, 2006; Pehar *et al.*, 2010) were recovered as before. Detergent-soluble and -insoluble fractions were prepared as described (Gan *et al.*, 2012). Briefly, cells were lysed in lysis buffer (50 mM Tris-HCl, pH 7.4, 150 mM NaCl, 2 mM EDTA, 1 mM dithiothreitol) completed with protease inhibitors (Roche) and 1% Triton™ X-100 (Buffer A), following centrifugation at 100 000*g* for 30 min at 4°C. Supernatants were recovered as Triton-soluble fractions. Pellets were washed with Buffer A three times, and then resuspended in lysis buffer containing Buffer A, 1% sodium dodecyl sulphate (SDS) and 0.5% sodium deoxycholate. After sonication and a brief spin down, the lysates were recovered as Triton-insoluble (SDS-soluble) fractions.

Differential detergent extraction of human SOD1 (hSOD1) from the spinal cord of early symptomatic mice was performed as previously described (Wang *et al.*, 2003). Briefly, tissue was lysed in TEN buffer (10 mM Tris-HCl pH 8.0, 1 mM EDTA, 100 mM NaCl, 0.5% NP-40 and protease inhibitors). After sonication the lysate was centrifuged at 100 000*g* for 5 min. The supernatant S1 was recovered as the non-ionic detergent soluble fraction. The pellet P1 was washed twice in TEN buffer by sonication and centrifuged at 100 000*g* for 5 min to obtain pellet P2. Pellet P2 was resuspended by sonication in TEN buffer supplemented with 0.5% sodium deoxycholate and 0.25% SDS. After centrifugation the supernatant was recovered as the non-ionic detergent insoluble fraction.

Protein concentration was measured by the bicinchoninic acid method (Pierce). Protein electrophoresis was performed on a NuPAGE® system using 4–12% Bis-Tris gels (Invitrogen).

The following primary antibodies were used: anti-Beta Amyloid (clone 6E10, 1:1000, Signet); anti-Amyloid Precursor Protein, C-Terminal (1:1000, Millipore); anti-phospho-PHF-tau (pSer202 + Thr205; clone AT8, 1:750, Thermo Scientific); anti-Tau (clone T46, 1:1000, Invitrogen); anti-Tau (3-repeat isoform RD3; clone 8E6/C11, 1:500, Millipore); anti-alpha Synuclein (clone LB509, 1:1000, Abcam); anti-Huntingtin (clone mEM48, 1:1000, Millipore); anti-hSOD1 (clone EPR1726, 1:10 000, Epitomics); anti-BACE1 (1:1000, Abcam); anti-p62 (1:1000, Cell Signaling); anti-actin (1:1000, Cell Signaling); anti-LC3B (1:1000, Cell Signaling); anti-ATG9A (1:1000, Epitomics); anti-acetylated lysine (1:100, Cell Signaling); anti-IDE (1:1000, Abcam); anti-NEP (1:1000, Millipore); anti-ATF6 (1:250, Imgenex); anti-Bip (1:1000, Cell Signaling); anti-phospho-eIF2a (1:1000, Cell Signaling); anti-eIF2a (1:1000, Cell Signaling); anti-phospho-PERK (1:200, Santa Cruz); anti-PERK (1:1000, Cell Signaling); anti-Calreticulin (1:1000, Abcam). Blots were visualized with goat anti-rabbit Alexa Fluor® 680-conjugated or anti-mouse Alexa Fluor® 800-conjugated secondary antibodies on infrared imaging (LICOR Odyssey Infrared Imaging System; LI-COR Biosciences), or with HRP-conjugated anti-mouse or anti-rabbit secondary antibodies on chemiluminescent detection (ImageQuant LAS4000; GE Healthcare).

## cDNA and plasmids

The plasmid containing human α-synuclein (A53T SYN) cDNA was a generous gift from Dr Jeffrey A. Johnson. This plasmid was used as a template to generate the cDNA of α-synuclein with an initiator methionine (M-A53T syn) or the signal peptide from human APP (SP-A53T syn) at the N-terminus. Primers for M-A53T syn were: 5′-AACCCAAGCT TGCCATGGATGTATTCATGAAAGGAC-3′ (forward) and 5′-AAGGCCTCGAGTCATTAGGCTTCAGGTTCGTAGTCT-3′ (reverse). Primers for SP-A53T syn were: 5′-AACCCA AGCTTGTCGCGATGCTGCCCGGTTTGGCACTGCTCCT GCTGGCCGCCTGGACGGCTCGGGCGATGGATGTATTC-ATGAAAGGAC-3′ (forward) and 5′-AAGGCCTCGAGTCAT TAGGCTTCAGGTTCGTAGTCT-3' (reverse). The PCR fragments were subsequently cloned (HindIII/XhoI) in vector pcDNA™3.1/*myc*-His (+) B (Invitrogen) resulting in plasmids M-A53T syn and SP-A53T syn.

The p5xATF6-GL3 plasmid was a gift from Ron Prywes (Addgene plasmid 11 976) (Wang *et al.*, 2000). For ATF6-luciferase reporter activity, MEFs were transfected with 5 μg promoter-reporter construct as well as the empty vector along with 0.1 μg of *Renilla* luciferase (Promega) by using Amaxa™ Basic Nucleofector™ Kit for Primary Mammalian Fibroblasts (Lonza). Firefly and *Renilla* luciferase activities were measured 24 h after transfection with a dual luciferase kit (Promega) and expressed as relative luciferase activity. Co-transfected *Renilla* luciferase was used to normalize for transfection efficiency (Ko and Puglielli, 2007).

*XBP1* quantitative PCR was carried out as described (Sha *et al.*, 2009). Primers for *XBP1* were: 5′>GAGTCCGCAG

CAGGTG>3′ (forward) and 5′>TCCAGAATGCCCAAAAG G>3′ (reverse). Primers for total *XBP1* were: 5′>ACATCT TCCCATGGACTCTG>3′ (forward) and 5′>TAGGTCCTT CTGGGTAGACC>3′ (reverse). Primers for *GAPDH* were: 5′> AGGTCGGTGTGAACGGATTTG>3′ (forward) and 5′> TGTAGACCATGTAGTTGAGGTCA>3′ (reverse).

## Histology and immunostaining

Histology and immunostaining techniques were described before (Pehar *et al.*, 2010; Peng *et al.*, 2014). The following primary antibodies were used: anti-phospho-PHF-Tau (clone AT8, 1:100, Thermo Scientific); anti-synaptophysin (clone YE269, 1:250, Abcam); anti-alpha Synuclein (clone LB509, 1:100, Abcam); anti-LC3B (1:100, Cell Signaling); anti-Beta Amyloid (clone 6E10, 1:100, Signet); anti-Beta Amyloid (clone 4E12, 1:100, MBL); anti-NeuN (clone A60, 1:100, EMD-Millipore). Secondary antibodies were Alexa 488- and Alexa 594-conjugated goat anti-rabbit and anti-mouse (5 μg/ml; Molecular Probes-Invitrogen). For phospho-PHF Tau-AT8 immunofluorescence, the secondary antibodies were biotin-labelled goat anti-mouse (5 μg/ml; Molecular Probes-Invitrogen) followed by Alexa 488- or Alexa 594-conjugated streptavidin (5 μg/ml; Molecular Probes-Invitrogen). Beta-amyloid staining was performed after pretreatment of tissue sections with 70% formic acid for 30 min. Processed slides were imaged on a Zeiss Axiovert 200 inverted fluorescent microscope.

## Statistical analysis

Data analysis was performed using GraphPad InStat 3.06 statistical software (GraphPad Software Inc.). Data are expressed as mean ± standard deviation (SD). Comparison of the means was performed using Student's *t*-test or one-way ANOVA followed by Tukey-Kramer multiple comparisons test. For lifespan assessment, data were analysed with the Kaplan-Meier lifespan test and log-rank test using GraphPad Prism version 4.0 (GraphPad Software). Differences were declared statistically significant if $P < 0.05$.

# Results

## AT-1 activity regulates the disposal of protein aggregates within the secretory pathway

To determine whether the increased activation of autophagy that results from reduced influx of acetyl-CoA into the ER preferentially degrades certain toxic protein aggregates, we used MEFs from AT-$1^{S113R/+}$ mice. AT-$1_{S113R}$ is a mutant version of AT-1 that is devoid of acetyl-CoA transport activity. As a result, AT-$1^{S113R/+}$ knock-in mice have increased activation of autophagy (Peng *et al.*, 2014). Both wild-type and AT-$1^{S113R/+}$ MEFs were transfected with A53T α-synuclein, a mutant version of α-synuclein that is associated with autosomal dominant Parkinson's disease (Polymeropoulos *et al.*, 1997). α-Synuclein has high propensity to aggregate and is found in Lewy bodies of sporadic and familial forms of Parkinson's disease, cortical dementia with Lewy bodies, as well as other forms of synucleinopathies (Galvin *et al.*, 2001). To discriminate between aggregates that form in the cytosol and in the secretory pathway we transfected the above MEFs with two different versions of α-synuclein: one that had an initiator methionine (M-A53T syn) to direct translation in the cytosol and one with a signal peptide (SP-A53T syn) to direct translation on the ER and insertion into the secretory pathway (Fig. 1A). To differentiate between soluble and aggregated species of α-synuclein, MEFs were sequentially lysed with Triton™ X-100 (for soluble/non-aggregated α-synuclein) and SDS (for aggregated α-synuclein) (Gan *et al.*, 2012).

The results show striking differences across the experimental set-up (Fig. 1B–F). Specifically, the levels of Triton-soluble α-synuclein were overall similar when comparing wild-type and AT-$1^{S113R/+}$ MEFs as well as M-A53T syn and SP-A53T syn (Fig. 1B and D) suggesting no overall differences in the aggregation of α-synuclein. There was also no significant difference when we compared levels of SDS-soluble M-A53T syn in wild-type and AT-$1^{S113R/+}$ MEFs (Fig. 1C and F) suggesting that the increased levels of autophagy in AT-$1^{S113R/+}$ MEFs do not influence the disposal of syn aggregates that form in the cytosol. In contrast, the levels of SDS-soluble SP-A53T syn were significantly decreased (Fig. 1E and F). To determine whether the reduced levels of SDS-soluble SP-A53T syn in AT-$1^{S113R/+}$ MEFs was simply due to a more efficient secretion of the protein aggregates, we immunoprecipitated α-synuclein from the media. However, as expected, the immunoprecipitation did not yield significant levels of the protein (Fig. 1G) confirming that AT-$1^{S113R/+}$ MEFs dispose of SP-A53T syn aggregates more efficiently. The increased efficiency in disposing of the toxic protein aggregates was accompanied by reduced cell toxicity, as assessed by determining LDH release in the media (Fig. 1H). Direct assessment of transfected cells revealed a marked co-localization of SP-A53T syn with LC3β, a commonly used marker of autophagy (Pehar *et al.*, 2012*b*; Peng *et al.*, 2014). We previously published that the autophagy flux is maintained in AT-$1^{S113R/+}$ (Peng *et al.*, 2014); therefore, the co-localization of SP-A53T syn with LC3β (Fig. 1I) and consequent reduced levels of SDS-soluble SP-A53T syn can be interpreted as a result of more efficient autophagy-mediated degradation of the aggregated protein. Finally, we blocked the progression of autophagy with bafilomycin (500 nM)/pepstatin A (10 μg/ml)/E64 (10 μg/ml) (BPE) and observed a significant increase in the levels of SDS-soluble SP-A53T syn (Fig. 1J), supporting our conclusion that autophagy is responsible for the clearance of SP-A53T syn aggregates.

When taken together the above results suggest that the increased autophagy activation described in AT-$1^{S113R/+}$ MEFs (Peng *et al.*, 2014) preferentially targets toxic protein aggregates that form within the secretory pathway.

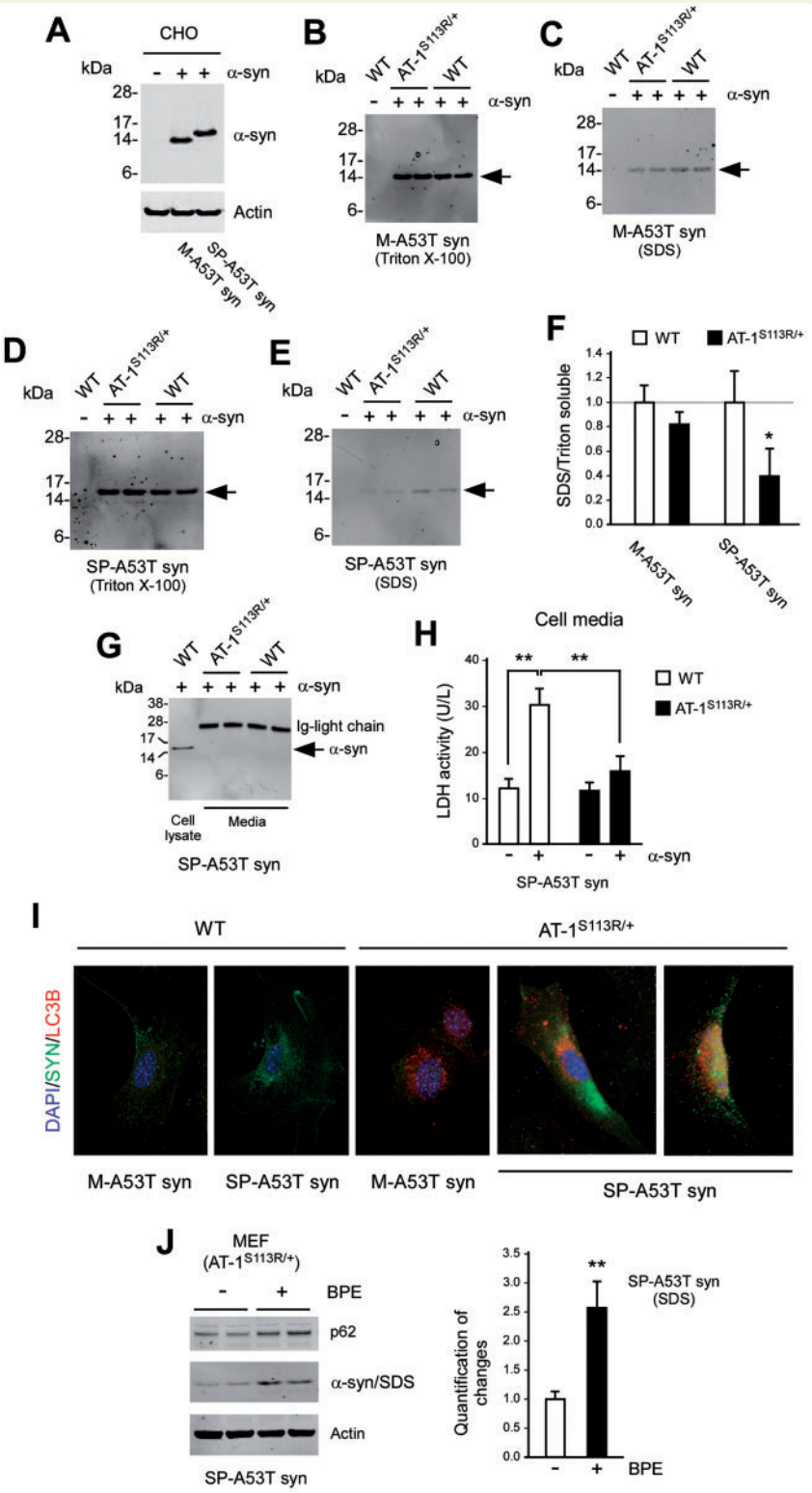


**Figure 1 Increased autophagy in AT-1$^{S113R/+}$ mice targets protein aggregates in the secretory pathway.** (**A**) Western blot showing the migration profile of M-A53T syn and SP-A53T syn. (**B–F**) MEFs from wild-type (WT) and AT-1$^{S113R/+}$ mice were transfected with mutant α-synuclein (A53T syn). Levels of soluble (Triton$^{TM}$ X-100) and insoluble/aggregated (SDS) A53T syn were detected by western blotting. M-A53T syn, α-synuclein with an initiator methionine; SP-A53T syn, α-synuclein with a signal peptide at the N-terminus. Selected images are shown in **B–E**, while quantification of changes is shown in **F**. Values are mean ± SD $^{*}P < 0.05$. Loading controls are shown in Supplementary Fig. 1. (**G**) Media from SP-A53T syn transfected MEFs were used to immunoprecipitate α-synuclein prior to western blotting. Total cell lysate served as positive control. (**H**) Lactated dehydrogenase (LDH) activity was assayed in the media of SP-A53T syn transfected MEFs. Values are mean ($n = 4$) ± SD. $^{**}P < 0.005$. (**I**) Immunolabelling showing co-localization of SP-A53T syn with LC3β puncta in AT-1$^{S113R/+}$ MEFs. As expected, LC3β displayed a

(continued)

## Reduced AT-1 activity in the mouse rescues Alzheimer's disease but not Huntington disease or amyotrophic lateral sclerosis

To confirm the above results in mouse models, we crossed AT-$1^{S113R/+}$ mice, which display reduced AT-1 transport activity and increased activation of autophagy in neurons (Peng *et al.*, 2014), with mouse models of Huntington's disease, amyotrophic lateral sclerosis, and Alzheimer's disease. Specifically, for Huntington's disease we used $mHtt^{Q160}$ (also known as R6/2) mice (Mangiarini *et al.*, 1996); for amyotrophic lateral sclerosis we used $hSOD1^{G93A}$ mice (Gurney *et al.*, 1994); and for Alzheimer's disease we used $APP_{695/swe}$ mice (Borchelt *et al.*, 1996; Pehar *et al.*, 2010). Both huntingtin (HTT) and superoxide dismutase 1 (SOD1) have an initiator methionine and are translated on cytosolic ribosomes. Protein aggregates in $mHtt^{Q160}$ are mainly observed in the nucleus (Mangiarini *et al.*, 1996; Davies *et al.*, 1997), whereas in $hSOD1^{G93A}$ they are observed in the cytosol, ER-Golgi compartment and mitochondria (Ferri *et al.*, 2006; Kikuchi *et al.*, 2006). In contrast to HTT and SOD1, the amyloid precursor protein (APP) is a type 1 membrane protein with a signal peptide at the N-terminus; it is translated on ER-bound ribosomes and inserts into the secretory pathway. Because of the topology of APP, the amyloid-β peptide that results from proteolytic cleavage of APP within the secretory pathway can only be released in the lumen of the organelle (or, eventually, secreted to the extracellular milieu) (Haass *et al.*, 1995; Cook *et al.*, 1997; Takami *et al.*, 2009). $APP_{695/swe}$ mice develop amyloid-β aggregates both inside and outside the neuronal cell body (Duyckaerts *et al.*, 2008).

Crossing $mHtt^{Q160}$ or $hSOD1^{G93A}$ mice with AT-$1^{S113R/+}$ mice did not rescue the Huntington's disease-like (Fig. 2) or the amyotrophic lateral sclerosis-like (Fig. 3) phenotypes. However, crossing $APP_{695/swe}$ with AT-$1^{S113R/+}$ mice resulted in a dramatic rescue of the Alzheimer's disease-like phenotype (Fig. 4). Specifically, we observed a drastic increase of the lifespan of the animals (Fig. 4A), reduced intraneuronal amyloid-β labelling (Fig. 4B), reduced levels of soluble amyloid-β aggregates (Fig. 4C and D), and improved synaptic plasticity, as assessed by long-term potentiation (Fig. 4E). To assess whether the phenotypic rescue was due to reduced generation of amyloid-β rather than to increased disposal of intracellular amyloid-β aggregates, we determined levels of BACE1 and APP in AT-$1^{S113R/+}$ mice. The results showed no significant changes on either protein (Fig. 4F, left). Consistently, no overall effect on APP processing was observed in $APP_{695/swe}$;AT-$1^{S113R/+}$ mice (Fig. 4F, right). Finally, to assess whether changes in amyloid-β were due to increased levels of amyloid-β-degrading proteases rather than to autophagy activation, we also determined levels of neprilysin and insulin-degrading enzyme, the two most prominent amyloid-β-degrading proteases (Wang *et al.*, 2006). However, no changes were observed (Fig. 4F, left).

In conclusion, the above results indicate that the increased activation of autophagy observed in AT-$1^{S113R/+}$ mice can selectively rescue the accumulation of amyloid-β toxic protein aggregates and the phenotype of $APP_{695/swe}$ mice. Together with Figs 1–3, they support the conclusion that a more efficient autophagy, as induced by targeting the ER-acetylation machinery, can resolve the accumulation of toxic protein aggregates that form within the secretory pathway but not those that form or accumulate in other compartments. Interestingly, AT-$1^{S113R/+}$ mice also show activation of unfolded protein response markers (Supplementary Fig. 2) supporting the general conclusion of improved proteostatic mechanisms acting in the secretory pathway.

## Biochemical inhibition of ATase1 and ATase2 in the mouse rescues the Alzheimer's disease-like phenotype

To confirm the results obtained with AT-$1^{S113R/+}$ mice, we decided to target the ER-based acetyltransferases (ATase1 or ATase2), which act downstream of AT-1 (Ko and Puglielli, 2009; Ding *et al.*, 2012). Specifically, we used recently identified and highly selective ATase1/ATase2 biochemical inhibitors (Ding *et al.*, 2012). The biochemical properties as well as mechanism of action of ATase1/ATase2 inhibitors (Compounds 9 and 19) have already been described (Ding *et al.*, 2012). The molecular characteristics of both compounds predicted excellent drug-like properties (Supplementary Table 1). Although Compound 19 displayed increased solubility in aqueous systems (Supplementary Table 2), Compound 9 had higher cLog*P* and was predicted to cross the blood–brain barrier with higher efficiency. As such, we decided to treat the animals with Compound 9. The highest concentration of the compound into the solid diet that could be reached without altering evident physical characteristics of the diet was 1.25 mg/g with multiple ethanol coating of

**Figure 1** Continued

diffuse cytosolic distribution in wild-type MEFs; puncta were only visible in AT-$1^{S113R/+}$ MEFs (Peng *et al.*, 2014). No co-localization of α-synuclein with LC3β puncta was observed in AT-$1^{S113R/+}$ MEFs transfected with M-A53T syn. (**J**) Western blot showing increased levels of SP-A53T syn aggregates following BPE treatment to arrest the autophagy flux. Increased levels of p62, an autophagy-cargo protein that is normally degraded as part of the autophagy process, served as a marker of successful blockage of autophagy. Representative images are in the *left* panel; quantitative changes of α-syn/SDS are in the *right* panel.

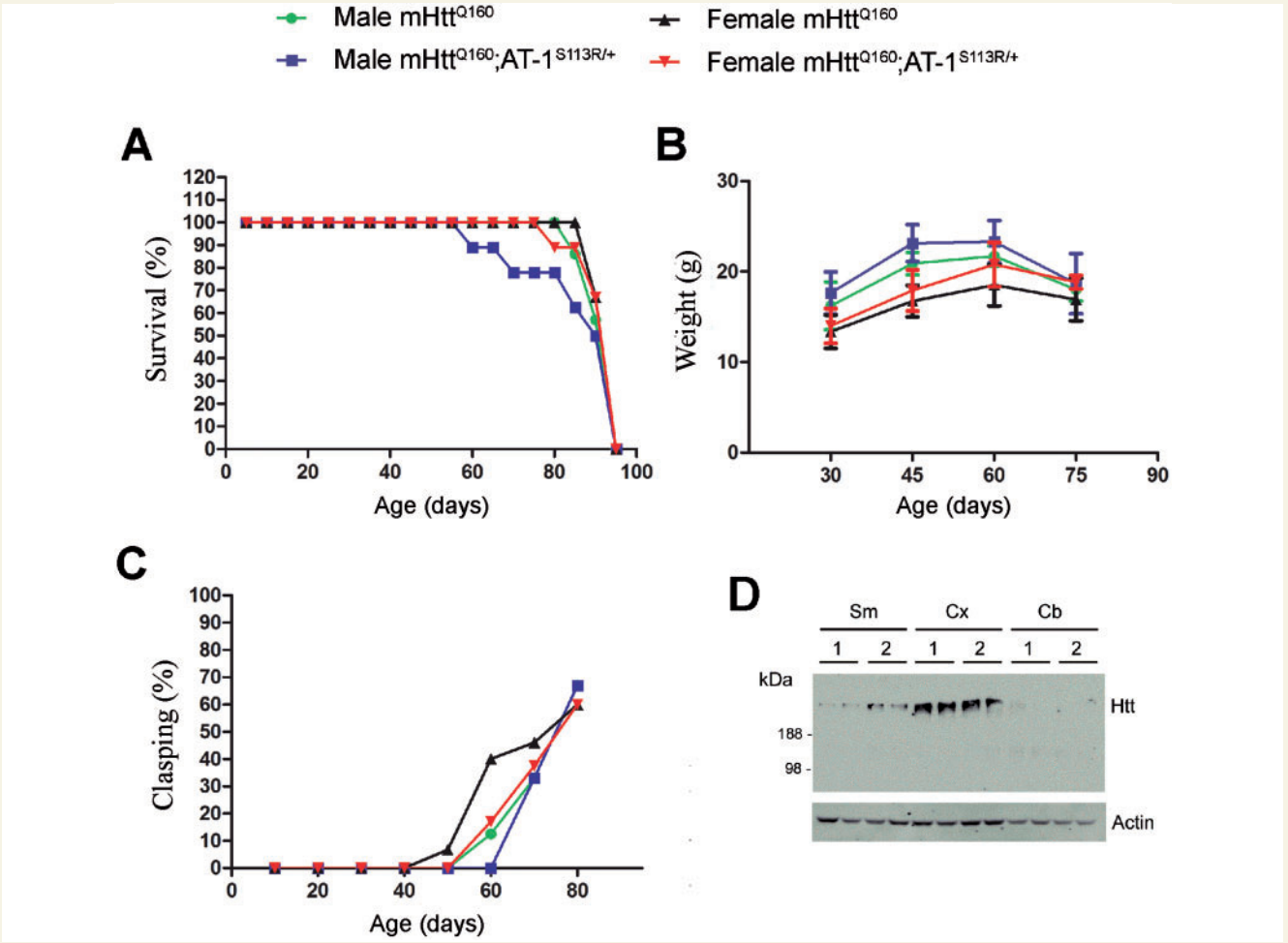


**Figure 2 Increased autophagy in AT-1$^{S113R/+}$ mice did not rescue the phenotype of mHtt$^{Q160}$ mice.** (**A–C**) Lifespan (**A**), body weight (**B**) and clasping (**C**) of indicated animals. Values in **B** are mean ± SD. Total numbers: females mHtt$^{Q160}$, *n* = 17; females mHtt$^{Q160}$;AT-1$^{S113R/+}$, *n* = 14; males mHtt$^{Q160}$, *n* = 18; males mHtt$^{Q160}$;AT-1$^{S113R/+}$, *n* = 18. (**D**) Western blot assessment of Htt aggregates in the striatum (Sm), cortex (Cx), and cerebellum (Cb). Lane 1: mHtt$^{Q160}$;AT-1$^{S113R/+}$ mice; Lane 2: mHtt$^{Q160}$ mice. Animals (males) were 2 months old when analysed.

sugar pellets and 2 mg/g with dustless extrusion of regular rodent pellets. For our studies we decided to use the dustless extrusion process (Supplementary Table 3). The compound was administered at the final dose of 50 mg/kg/day.

To assess whether the compound was indeed able to reach the CSF, an initial group of mice received the compound for 1 week prior to collection of the CSF. Treatment was limited to 1 week, which is usually sufficient to reach equilibrium in biological fluids (Ito *et al.*, 1998; Singh, 2006; Houston and Galetin, 2008). Concentration and duration of the treatment was based on previous studies with drug-like compounds having similar mass and solubility properties (Ito *et al.*, 1998; Singh, 2006; Houston and Galetin, 2008). Assessment of the CSF by mass spectrometry identified the compound in all treated animals but not in control (untreated) animals, confirming our early prediction (Supplementary Fig. 3).

In light of these results we decided to begin a long-term study with APP$_{695/swe}$ mice. The animals received Compound 9 throughout the entire duration of the study. They develop Alzheimer's disease-like neuropathology in an age-dependent fashion (reviewed in Duyckaerts *et al.*, 2008; Lalonde *et al.*, 2012); therefore, different disease-relevant manifestations were studied at different time points (Fig. 5A). When assessed at 5 months of age, APP$_{695/swe}$ mice treated with Compound 9 displayed reduced levels of BACE1 (Fig. 5B) and soluble amyloid-β (Fig. 5C). BACE1 is the rate-limiting enzyme for the generation of amyloid-β from APP and a well characterized substrate of the ATases (Ko and Puglielli, 2009; Ding *et al.*, 2012, 2014). Thus, the reduced levels of BACE1 indicate successful inhibition of the ATases in the brain. APP$_{695/swe}$ mice treated with Compound 9 also displayed reduced levels of p62, reduced LC3βI/LC3βII ratio, and increased LC3βII/actin ratio in the brain (Fig. 5D and E). The induction of autophagy is

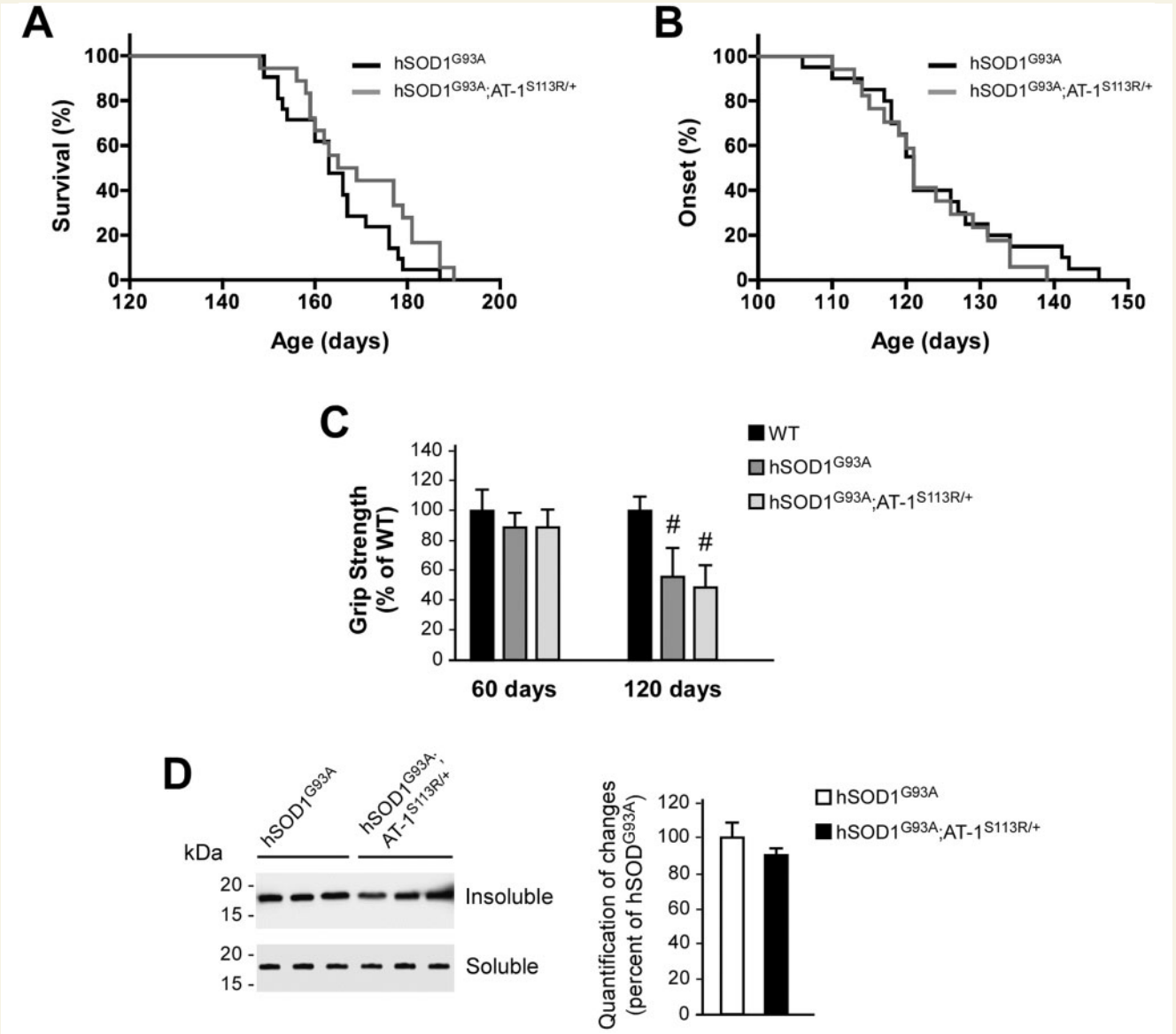


**Figure 3 Increased autophagy in AT-1$^{S113R/+}$ mice did not rescue the phenotype of hSOD1$^{G43A}$ mice.** (**A**) Median survival in hSOD1$^{G93A}$ (163 days; $n = 21$) and hSOD1$^{G93A}$;AT-1$^{S113R/+}$ (167 days; $n = 18$) mice. (**B**) Median onset of symptoms in hSOD1$^{G93A}$ (121 days; $n = 20$) and hSOD1$^{G93A}$;AT-1$^{S113R/+}$ (121 days; $n = 17$) mice. (**C**) Hindlimb grip-strength in wild-type ($n = 15$), hSOD1$^{G93A}$ ($n = 20$), and hSOD1$^{G93A}$;AT-1$^{S113R/+}$ ($n = 16$) at 60 and 120 days. No significant difference was observed between hSOD1$^{G93A}$ and hSOD1$^{G93A}$;AT-1$^{S113R/+}$ mice. Average grip-strength in wild-type mice was 100.0 ± 9.8 *gf* for males and 93.1 ± 16.2 *gf* for females at 60 days; and 103.2 ± 11.2 *gf* for males and 101.9 ± 9.1 *gf* for females at 120 days. Data are mean ± SD. $^{\#}P < 0.0005$ (from wild-type). (**D**) Western blot against hSOD1 in the spinal cord of early symptomatic hSOD1$^{G93A}$ and hSOD1$^{G93A}$;AT-1$^{S113R/+}$ mice after differential detergent extraction. Non-ionic detergent insoluble hSOD1 (insoluble; P2 pellet) is shown in the *upper* panel. The *lower* panel shows hSOD1 in the NP-40 soluble fraction (soluble; S1 supernatant).

normally accompanied by reduced levels of p62, an autophagosome-associated protein that is degraded as a result of the autophagic process, as well as conversion of LC3βI into the autophagosome-bound LC3βII (Mizushima *et al.*, 2010). As such, the results displayed in Fig. 5D and E suggest that, similar to mice with reduced AT-1 activity (AT-1$^{S113R/+}$) (Peng *et al.*, 2014), Compound 9-treated animals also display increased autophagy. This conclusion was further confirmed by the identification of LC3β staining in neurons of APP$_{695/swe}$ mice treated with Compound 9 (Fig. 5F). Importantly, LC3β autophagy puncta were observed throughout the brain and showed complete overlap with NeuN (Fig. 5F). No LC3β puncta were observed in mice fed the control diet. We previously published that the induction of autophagy that results from the inhibition of ER acetylation depends on the acetylation status of ATG9A; specifically, reduced acetylation stimulates while increased acetylation blocks the induction of autophagy

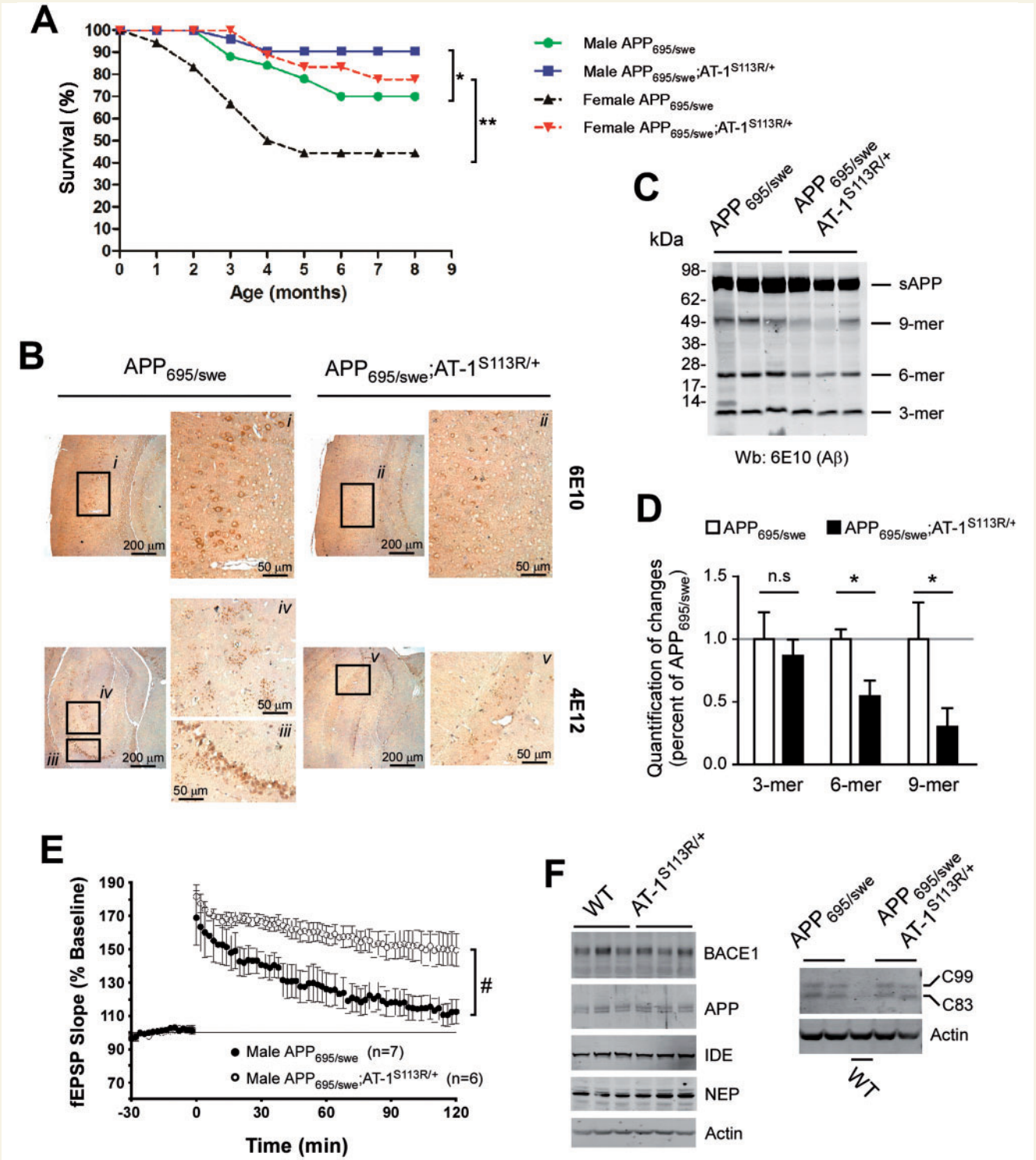


**Figure 4 Increased autophagy in AT-1$^{S113R/+}$ mice rescued the phenotype of APP$_{695/swe}$ mice.** (**A**) Lifespan of indicated mice (Kaplan-Meier analysis). Numbers used: females APP$_{695/swe}$, $n$ = 18; females APP$_{695/swe}$;AT-1$^{S113R/+}$, $n$ = 18; males APP$_{695/swe}$, $n$ = 25; males APP$_{695/swe}$;AT-1$^{S113R/+}$, $n$ = 26. *$P < 0.05$; **$P < 0.005$. Lifespan of APP$_{695/swe}$ mice was similar to already published data (reviewed in Lalonde *et al.*, 2012). (**B**) Immunohistochemistry for intracellular amyloid-β aggregates. Two anti-amyloid-β antibodies were used (6E10 and 4E12). High magnification of indicated areas is shown. Animals (males) were 8 months old when analysed. (**C**) Western blot of extracellular amyloid-β oligomers in brain homogenate. Indicated bands correspond to already characterized amyloid-β oligomers (Lesne *et al.*, 2006; Pehar *et al.*, 2010). soluble APP (sAPP) is also indicated. Animals (males) were 8 months old when analysed. (**D**) Quantification of major amyloid-β reactive species shown in **C**. Values are mean ($n$ = 3) ± SD. *$P < 0.05$. (**E**) Long-term potentiation induction in hippocampal slices. APP$_{695/swe}$ mice lack the late component of long-term potentiation; these deficits were rescued by the AT-1 haploinsufficiency. Typical long-term potentiation of wild-type/non-transgenic animals is shown in Fig. 6C. Values are mean ± SD. #$P < 0.0005$. (**F**) Western blot showing levels of BACE1, APP, NEP, IDE, C99 and C83.

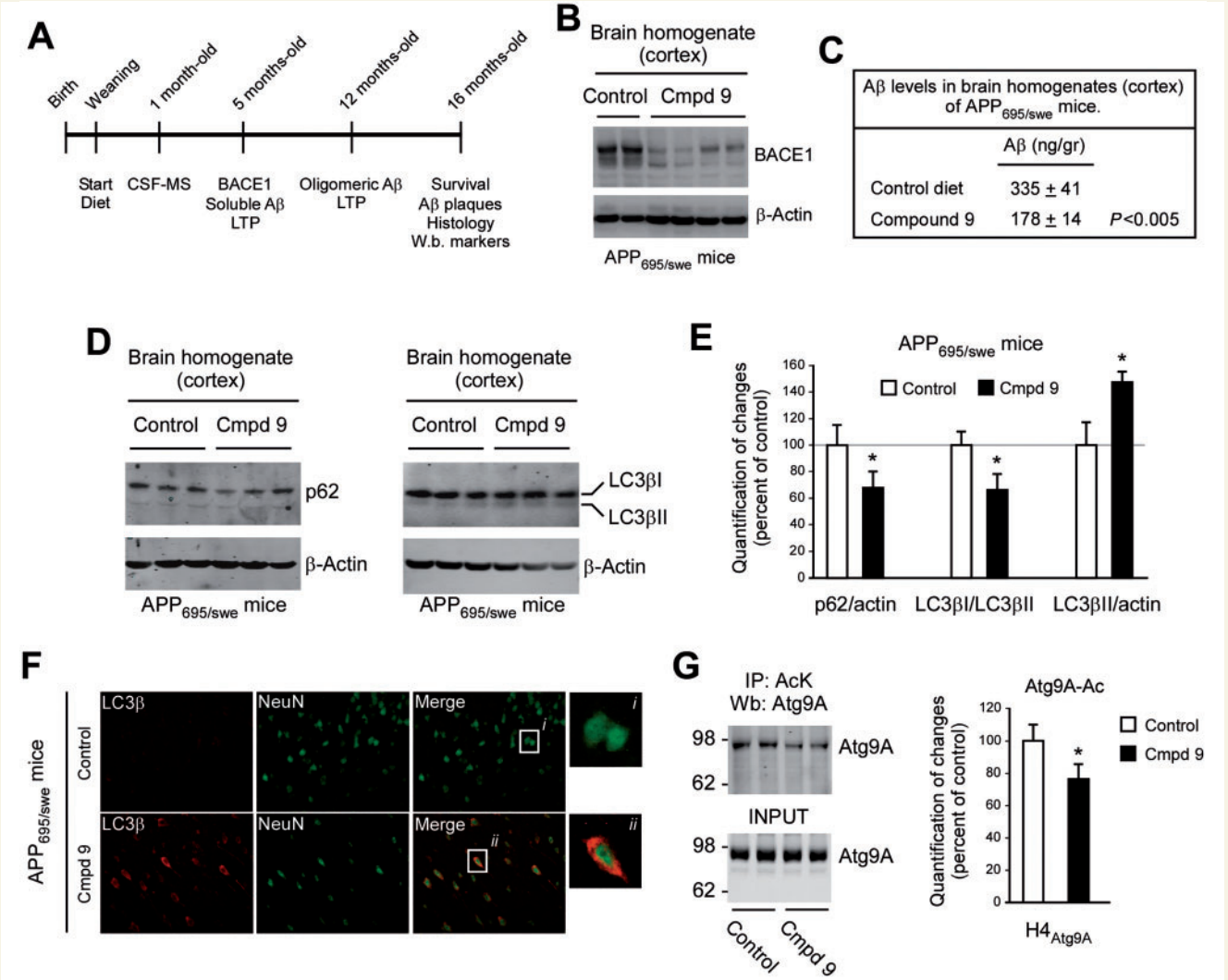


**Figure 5 Biochemical inhibition of ATase1 and ATase2 rescued the phenotype of $APP_{695/swe}$ mice (males) displayed at 5 months of age.** (**A**) Schematic view of the study plan. Description is in the text. (**B**) Western blot analysis of BACE1 levels. Control = control diet; Cmpd 9 = Compound 9. (**C**) ELISA determination of amyloid-β levels. Values are mean ($n = 7$) ± SD. (**D**) Western blot assessment of commonly-used autophagy markers. (**E**) Quantification of results shown in **D**. Values are mean ($n = 6$) ± SD. $^*P < 0.05$. (**F**) Immunolabelling showing LC3β puncta in Compound 9-treated animals (brain cortex). LC3β positive labelling co-localizes with NeuN staining. (**G**) Western blot showing the acetylation status of ATG9A following Compound 9 treatment (10 μM; 3 days; $n = 4$) of ATG9A overexpressing H4 cells ($H4_{Atg9A}$). Immunoprecipitation (IP) was performed with an anti-acetylated lysine antibody (AcK). INPUT is also shown. Levels of acetylated ATG9A (Atg9A-Ac) were normalized to the INPUT.

(Pehar and Puglielli, 2013; Peng *et al.*, 2014). To confirm that Compound 9 acts through the same molecular pathway, we determined the acetylation status of ATG9A in cells treated with Compound 9. We observed a significant reduction in acetylated ATG9A (Fig. 5G), thus confirming our overarching conclusions.

At 12 months of age, $APP_{695/swe}$ mice display high molecular mass amyloid-β species (oligomers); they originate from the aggregation of the monomeric peptide and are highly toxic (Cleary *et al.*, 2005; Lesne *et al.*, 2006; Pehar *et al.*, 2010). Treatment with Compound 9 resulted in a marked decrease in the levels of amyloid-β oligomers observed (Fig. 6A and B). As expected, $APP_{695/swe}$ mice displayed a significant defect in the late phase of long-term potentiation, which is an indication of impaired synaptic plasticity; however, this defect was completely rescued by Compound 9 (Fig. 6C). Changes in long-term potentiation were not observed when the compound was administered to control (non-transgenic) mice (Supplementary Fig. 4C) indicating that treatment does not affect intrinsic synaptic activities but only rescues disease-relevant features.

When assessed at 16 months of age, $APP_{695/swe}$ mice displayed severe amyloid-β pathology, as indicated by the high number of plaque formation throughout the brain parenchyma; this phenotype, which is typical of Alzheimer's disease, was rescued by Compound 9 (Fig. 7A). Histological

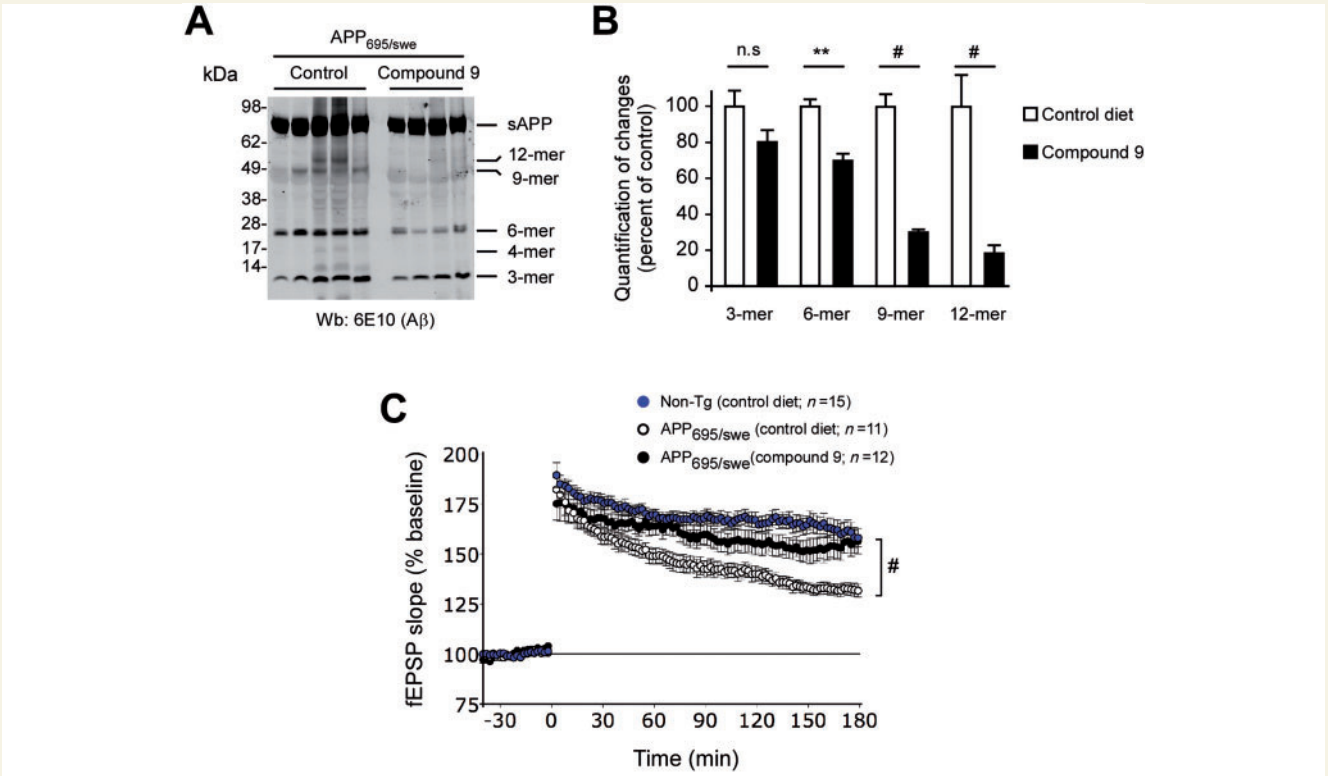


**Figure 6 Biochemical inhibition of ATase1 and ATase2 rescued the phenotype of $APP_{695/swe}$ mice (males) displayed at 12 months of age.** (**A**) Western blot of extracellular amyloid-β oligomers in brain homogenate. Indicated bands correspond to already characterized amyloid-β oligomers (Lesne *et al.*, 2006; Pehar *et al.*, 2010). Band specificity and loading controls are shown in Supplementary Fig. 4A and B. (**B**) Quantification of major amyloid-β reactive species shown in (**A**). $^{**}P < 0.005$; $^{\#}P < 0.0005$. (**C**) Long-term potentiation induction in hippocampal slices of indicated animals. Values are mean ± SD. $^{\#}P < 0.0005$.

assessment also revealed reduced phospho-tau immunostaining, which was paralleled by increased synaptophysin labelling (Fig. 7B). Hyper-phosphorylation of tau and loss of the 'synaptic mesh' are typical features of Alzheimer's disease. The drastic effect on levels of tau phosphorylation was also observed by immunoblotting (Fig. 7C and D). In addition to reduced levels of phospho-tau, western blot assessment of brain homogenates also detected a slight decrease in the C-terminal fragments of APP, C99 and C83 (Fig. 7C and D). Untreated $APP_{695/swe}$ mice displayed reduced survival with 50% lethality at ~14 months of age. However, this early lethality was completely rescued by Compound 9 treatment resulting in a normal lifespan (Fig. 7E and F). Routine histological assessment of peripheral tissues (Supplementary Fig. 5) detected no evidence of toxicity associated with the treatment.

When taken together, the above results indicate that biochemical inhibition of ATase1/ATase2 can rescue the Alzheimer's disease-like phenotype displayed by $APP_{695/swe}$ mice in the absence of evident toxicity. This effect is likely due to a combination of events, among which reduced generation and increased disposal of toxic amyloid-β aggregates through autophagy.

# Discussion

Here, we show that Nε-lysine acetylation in the ER lumen regulates normal proteostasis of the secretory pathway. We also report that inhibition of ER-acetylation can rescue diseases associated with accumulation of toxic protein aggregates that form within the secretory pathway. These conclusions were reached by using *ex vivo* and *in vivo* models. The latter included mice deficient in AT-1 transport activity as well as mice treated with ATase1/ATase2 specific inhibitors.

The major difference between $AT\text{-}1^{S113R/+}$ and Compound 9-treated animals was in BACE1 and APP metabolism. Indeed, both mouse models displayed increased autophagy (see Figs 4 and 5 and Peng *et al.*, 2014), but only Compound 9-treated animals displayed reduced levels of BACE1 and reduced processing of APP (compare Fig. 4 with Figs 5 and 7). The likely explanation is in the kinetics of acetylation of individual substrates. Specifically, the levels of acetylCoA influx into the ER of $AT\text{-}1^{S113R/+}$ mice are sufficiently low to affect the acetylation of ATG9A and stimulate autophagy (Peng *et al.*, 2014), but not low enough to affect the levels of BACE1. Direct

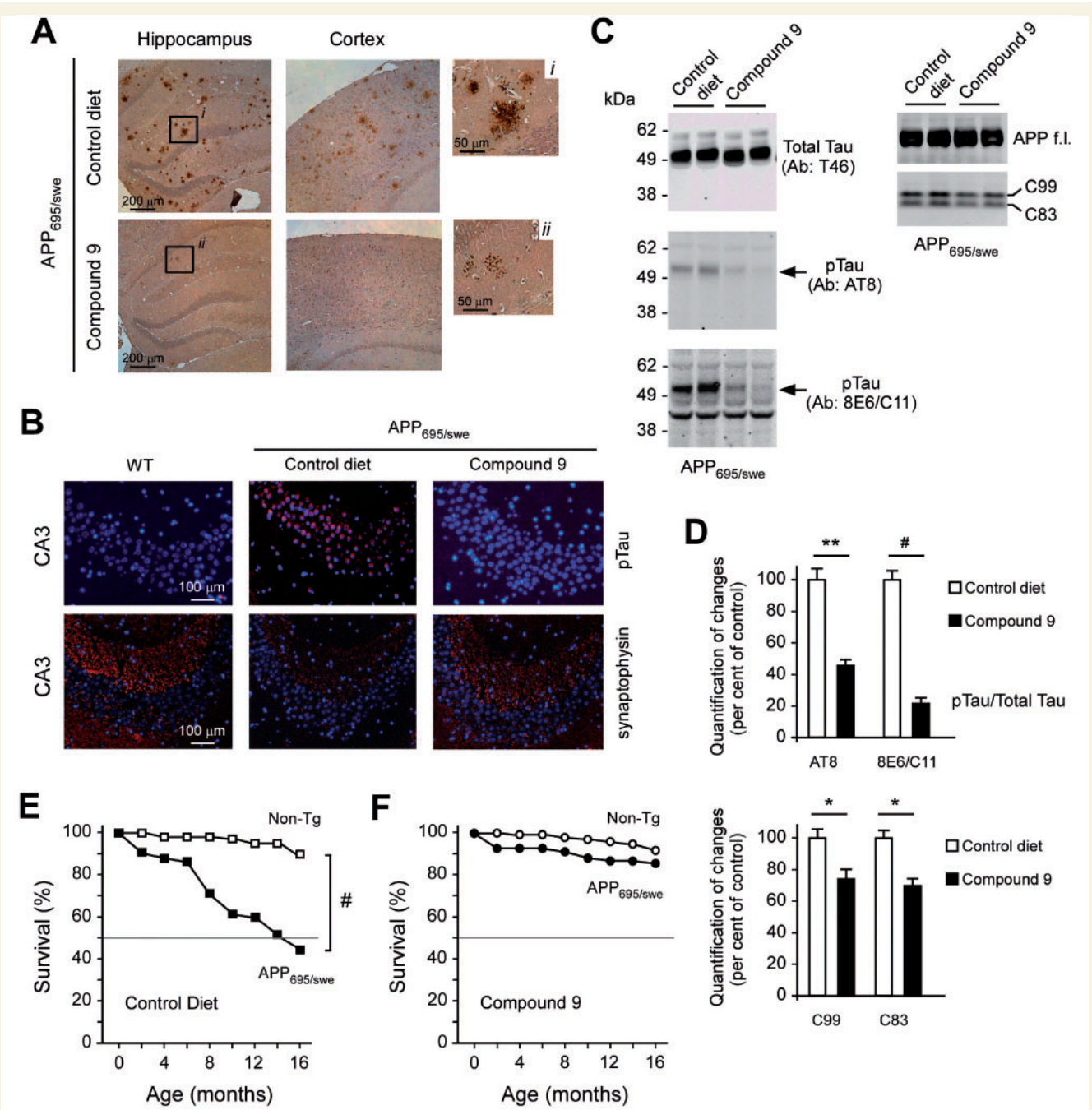


**Figure 7 Biochemical inhibition of ATase1 and ATase2 rescued the phenotype of $APP_{695/swe}$ mice (males) displayed at 16 months of age.** (**A**) Immunohistochemistry to visualize amyloid plaques. High magnification of indicated areas is shown. (**B**) Immunolabelling for phosphorylated tau (pTau) and synaptophysin in the CA3 region of the hippocampus. (**C**) Brain homogenate (cortex) of indicated animals were analysed by western blot. Levels of phosphorylated tau (pTau) were determined with two different phospho-specific antibodies (AT8 and 8EC6/C11). Total Tau and full-length APP (APP f.l.) served as internal loading controls. Only levels of pTau and C99/C83 showed significant changes (**D**). (**D**) Quantification of pTau, C99, and C83 levels shown in **C**. Values are mean ± SD. $^{*}P < 0.05$; $^{**}P < 0.005$; $^{\#}P < 0.0005$. (**E** and **F**) Lifespan of wild-type/non-transgenic (Non-Tg) and $APP_{695/swe}$ mice (males) fed a control diet (**E**) or a diet containing Compound 9 (**F**). Kaplan-Meier analysis is shown. Numbers used were as follows: Non-Tg, control diet, $n = 30$; Compound 9, $n = 39$); $APP_{695/swe}$ (control diet, $n = 26$; Compound 9, $n = 30$). $^{\#}P < 0.0005$.

inhibition of the transferases, instead, is able to affect a larger number of substrates, thus reducing the generation of amyloid-β but also stimulating the autophagy-mediated disposal of amyloid-β aggregates. The existence of different substrate-saturation kinetics for ER acetylation is supported by published studies (Costantini *et al.*, 2007; Mak *et al.*, 2014). Although it is impossible to dissect the specific contribution of the above mechanisms in the Compound 9-

treated model, the results displayed in Figs 1 and 4 clearly suggest that the autophagy-mediated disposal mechanism is an important component. Obviously, it is also possible that additional and not yet characterized effects of Compound 9 (such as regulation of proteasome activity) might contribute in the phenotypic correction.

One of the functions of the ER is to ensure that nascent membrane and secreted polypeptides fold correctly. Incorrectly folded polypeptides, which failed quality control, must be sorted and disposed of. For this purpose, transient modifications have been designed to select correctly folded and unfolded/misfolded polypeptides. Studies conducted with two well-characterized substrates of the ATases, BACE1 and CD133, suggest that Nε-lysine acetylation might be part of normal quality control to select correctly folded polypeptides (Costantini *et al*., 2007; Ko and Puglielli, 2009; Ding *et al*., 2014; Mak *et al*., 2014). Indeed, a block in the acetylation of both BACE1 and CD133 resulted in the nascent protein being retained and disposed of in the early secretory pathway (Costantini *et al*., 2007; Mak *et al*., 2014). Recognition features that control the activity of the acetyltransferases as well as the identity of all ATase1- and ATase2-specific substrates still remain to be determined.

Another important function of the ER is to dispose of unfolded/misfolded polypeptides as part of ER-associated degradation. Monomeric proteins that can be retro-translocated to the cytosol across the ER membrane are preferentially degraded by the proteasome (Trombetta and Parodi, 2003). In contrast, large protein aggregates are mostly dealt with by expanding the ER and activating autophagy (Bernales *et al*., 2006; Ogata *et al*., 2006; Ding *et al*., 2007; Axe *et al*., 2008). Therefore, autophagy is as an essential cellular function that ensures disposal of unwanted material. This is particularly important for neurons (Klionsky, 2006; Komatsu *et al*., 2006, 2007; Lee, 2009; Pehar and Puglielli, 2013). If unchecked, autophagy can become terminal. Indeed, aberrant induction of autophagy in AT-$1^{S113R/+}$ mice resulted in a severe phenotype (Peng *et al*., 2014). However, compelling data also indicate that the autophagy machinery can be manipulated to improve the disposal of toxic protein aggregates. The same data also indicate that increased levels of autophagy, which are pathogenic in wild-type mice in the absence of toxic protein aggregates, can be beneficial in mouse models of diseases characterized by increased accumulation of toxic protein aggregates (van Dellen *et al*., 2000; Pickford *et al*., 2008; Hetz *et al*., 2009; Madeo *et al*., 2009; Bhuiyan *et al*., 2013).

Autophagy can be induced through different mechanisms, and to respond to different insults (Klionsky, 2006; Lee, 2009; Pehar and Puglielli, 2013). As such, it is likely that a certain degree of specificity exists. The studies performed with α-synuclein (Fig. 1) indicate that the increased levels of autophagy observed in AT-$1^{S113R/+}$ mice affect the disposal of protein aggregates that form within the secretory pathway but not in other compartments. The same conclusions were reached by using mouse models of disease (Figs 2–4). Whether there are more precise spatial restrictions within the secretory pathway is unclear. Previous data have shown that the acetylation status of ATG9A is crucial for the induction of autophagy downstream of AT-1 (Pehar *et al*., 2012*b*; Peng *et al*., 2014). ATG9A is the only membrane-bound autophagy protein and can be recruited to LC3β-positive autophagosomes from different locations, including the ER, the Golgi apparatus, and even the plasma membrane (Young *et al*., 2006; Ohashi and Munro, 2010; Tamura *et al*., 2010; Puri *et al*., 2013; Bejarano *et al*., 2014). Therefore, it will be difficult to delineate possible spatial restrictions by targeting ATG9A. A similar limitation exists with amyloid-β, which can be generated in different cellular compartments, including the ER and the Golgi apparatus (Haass *et al*., 1995; Cook *et al*., 1997; Takami *et al*., 2009). Interestingly, autophagy deficiency, as caused by genetic disruption of ATG7, leads to aberrant accumulation of intracellular amyloid-β in the early secretory pathway and results in an exacerbated neurodegenerative phenotype (Nilsson *et al*., 2013, 2015).

It is also worth noting that the role of autophagy in neurodegenerative mouse models is not completely straightforward. Indeed, alterations of specific regulatory steps of the autophagy process, including impaired fusion of autophagosomes with lysosomes, inefficient degradation of the cargo, or defective cytosolic cargo recognition, have been described in certain models causing autophagy induction to be detrimental (Marino *et al*., 2011; Vidal *et al*., 2014). Although activation of autophagy has been shown to be protective in models of Alzheimer's disease, Huntington's disease, and amyotrophic lateral sclerosis (reviewed in Vidal *et al*., 2014), the final outcome on disease progression appears to depend on the specific regulatory step being targeted and the pathological context. Accordingly, in mutant hSOD1 amyotrophic lateral sclerosis mouse models, activation of autophagy by rapamycin has detrimental or no effect, while activation of autophagy by trehalose treatment or downregulation of XBP1 decreases hSOD1 aggregates and enhances motor neuron survival (Zhang *et al*., 2011; Bhattacharya *et al*., 2012; Vidal *et al*., 2012; Castillo *et al*., 2013). On the other hand, haploinsufficiency of beclin 1, a key player in the initiation steps of autophagy, appears to be beneficial by reversing autophagy alterations induced by an abnormal interaction of mutant hSOD1 with the beclin 1/BCL-$X_L$ complex (Nassif *et al*., 2014). Thus, we cannot exclude the possibility that the presence of defects in other autophagy regulatory steps counteract the protective effect of increasing ER proteostasis in the Huntington's disease and amyotrophic lateral sclerosis mouse models used here. It is also important to consider that, although hSOD1 lacks a signal peptide, it can translocate into the secretory pathway through a not well characterized mechanism that involves ATP consumption (Urushitani *et al*., 2008). Indeed, hSOD1 aggregates have been described within the secretory pathway (Urushitani *et al*., 2008). Thus, in the case of $hSOD1^{G93A}$, the disposal of hSOD1 aggregates within the secretory pathway might account for the small reduction in

hSOD1 aggregates observed in the spinal cord of early symptomatic hSOD1$^{G93A}$;AT-1$^{S113R/+}$ mice (Fig. 3). If this is true, then we could assume that the toxicity of mutant hSOD1 in other cellular compartments prevented rescue of the phenotype. In the case of Huntington's disease models, mutant huntingtin has been reported to alter the activity of the ubiquitin-proteasome system, thus interfering with both cytosolic protein degradation and ER-associated degradation (Duennwald and Lindquist, 2008; Leitman *et al.*, 2013). The inhibition of ER-associated degradation promotes the accumulation of misfolded proteins in the ER and the subsequent activation of the unfolded protein response. However, we observed that the increased autophagy-dependent ER-associated degradation [ERAD(II)] associated with haploinsufficiency of AT-1 in the double transgenic mHtt$^{Q160}$;AT-1$^{S113R/+}$ mice is not sufficient to revert the phenotype.

In conclusion, our results indicate that there is significant specificity in the induction of autophagy; they also support therapies targeting ER acetyltransferases, ATase1 and ATase2, for a specific subset of chronic degenerative diseases.

## Acknowledgements

The authors thank Dr Jeff Johnson for the α-synuclein construct and Dr Ron Prywes for the p5xATF6-GL3 plasmid.

## Funding

This work was supported by: VA Merit Award (BX001638), NIH (NS094154 and GM103542), and Thome Memorial Foundation. R.H. was supported by a National Science Foundation Graduate Research Fellowship.

## Supplementary material

Supplementary material is available at *Brain* online.

## References

Axe EL, Walker SA, Manifava M, Chandra P, Roderick HL, Habermann A, et al. Autophagosome formation from membrane compartments enriched in phosphatidylinositol 3-phosphate and dynamically connected to the endoplasmic reticulum. J Cell Biol 2008; 182: 685–701.

Bhattacharya A, Bokov A, Muller FL, Jernigan AL, Maslin K, Diaz V, et al. Dietary restriction but not rapamycin extends disease onset and survival of the H46R/H48Q mouse model of ALS. Neurobiol Aging 2012; 33: 1829–32.

Bejarano E, Yuste A, Patel B, Stout RF, Jr., Spray DC, Cuervo AM. Connexins modulate autophagosome biogenesis. Nat Cell Biol 2014; 16: 401–14.

Bernales S, McDonald KL, Walter P. Autophagy counterbalances endoplasmic reticulum expansion during the unfolded protein response. PLoS Biol 2006; 4: e423.

Bhuiyan MS, Pattison JS, Osinska H, James J, Gulick J, McLendon PM, et al. Enhanced autophagy ameliorates cardiac proteinopathy. J Clin Invest 2013; 123: 5284–97.

Borchelt DR, Thinakaran G, Eckman CB, Lee MK, Davenport F, Ratovitsky T, et al. Familial Alzheimer's disease-linked presenilin 1 variants elevate Abeta1-42/1-40 ratio *in vitro* and *in vivo*. Neuron 1996; 17: 1005–13.

Castillo K, Nassif M, Valenzuela V, Rojas F, Matus S, Mercado G, et al. Trehalose delays the progression of amyotrophic lateral sclerosis by enhancing autophagy in motoneurons. Autophagy 2013; 9: 1308–20.

Choudhary C, Kumar C, Gnad F, Nielsen ML, Rehman M, Walther TC, et al. Lysine acetylation targets protein complexes and co-regulates major cellular functions. Science 2009; 325: 834–40.

Cleary JP, Walsh DM, Hofmeister JJ, Shankar GM, Kuskowski MA, Selkoe DJ, et al. Natural oligomers of the amyloid-beta protein specifically disrupt cognitive function. Nat Neurosci 2005; 8: 79–84.

Cook DG, Forman MS, Sung JC, Leight S, Kolson DL, Iwatsubo T, et al. Alzheimer's A beta(1-42) is generated in the endoplasmic reticulum/intermediate compartment of NT2N cells. Nat Med 1997; 3: 1021–3.

Costantini C, Ko MH, Jonas MC, Puglielli L. A reversible form of lysine acetylation in the ER and Golgi lumen controls the molecular stabilization of BACE1. Biochem J 2007; 407: 383–95.

Costantini C, Scrable H, Puglielli L. An aging pathway controls the TrkA to p75(NTR) receptor switch and amyloid beta-peptide generation. EMBO J 2006; 25: 1997–2006.

Costantini C, Weindruch R, Della Valle G, Puglielli L. A TrkA-to-p75NTR molecular switch activates amyloid beta-peptide generation during aging. Biochem J 2005; 391: 59–67.

Davies SW, Turmaine M, Cozens BA, DiFiglia M, Sharp AH, Ross CA, et al. Formation of neuronal intranuclear inclusions underlies the neurological dysfunction in mice transgenic for the HD mutation. Cell 1997; 90: 537–48.

Ding WX, Ni HM, Gao W, Hou YF, Melan MA, Chen X, et al. Differential effects of endoplasmic reticulum stress-induced autophagy on cell survival. J Biol Chem 2007; 282:4702–10.

Ding Y, Dellisanti CD, Ko MH, Czajkowski C, Puglielli L. The endoplasmic reticulum-based acetyltransferases, ATase1 and ATase2, associate with the oligosaccharyl-transferase to acetylate correctly folded polypeptides. J Biol Chem 2014; 289: 32044–55.

Ding Y, Ko MH, Pehar M, Kotch F, Peters NR, Luo Y, et al. Biochemical inhibition of the acetyltansferases ATase1 and ATase2 reduces b-secretase (BACE1) levels and Ab generation. J Biol Chem 2012; 287: 8424–33.

Duennwald ML, Lindquist S. Impaired ERAD and ER stress are early and specific events in polyglutamine toxicity. Genes Dev 2008; 22: 3308–19.

Duyckaerts C, Potier MC, Delatour B. Alzheimer disease models and human neuropathology: similarities and differences. Acta Neuropathol 2008; 115: 5–38.

Eisenberg T, Schroeder S, Andryushkova A, Pendl T, Kuttner V, Bhukel A, et al. Nucleocytosolic depletion of the energy metabolite acetyl-coenzyme a stimulates autophagy and prolongs lifespan. Cell Metab 2014; 19: 431–44.

Ferri A, Cozzolino M, Crosio C, Nencini M, Casciati A, Gralla EB, et al. Familial ALS-superoxide dismutases associate with mitochondria and shift their redox potentials. Proc Natl Acad Sci USA 2006; 103: 13860–5.

Frake RA, Ricketts T, Menzies FM, Rubinsztein DC. Autophagy and neurodegeneration. J Clin Invest 2015; 125: 65–74.

Galvin JE, Lee VM, Trojanowski JQ. Synucleinopathies: clinical and pathological implications. Arch Neurol 2001; 58: 186–190.

Gan L, Vargas MR, Johnson DA, Johnson JA. Astrocyte-specific overexpression of Nrf2 delays motor pathology and synuclein

aggregation throughout the CNS in the alpha-synuclein mutant (A53T) mouse model. J Neurosci 2012; 32: 17775–87.
Gurney ME, Pu H, Chiu AY, Dal Canto MC, Polchow CY, Alexander DD, et al. Motor neuron degeneration in mice that express a human Cu,Zn superoxide dismutase mutation. Science 1994; 264: 1772–5.
Haass C, Lemere CA, Capell A, Citron M, Seubert P, Schenk D, et al. The Swedish mutation causes early-onset Alzheimer's disease by beta-secretase cleavage within the secretory pathway. Nat Med 1995; 1: 1291–6.
Hetz C, Thielen P, Matus S, Nassif M, Court F, Kiffin R, et al. XBP-1 deficiency in the nervous system protects against amyotrophic lateral sclerosis by increasing autophagy. Genes Dev 2009; 23: 2294–306.
Houston JB, Galetin A. Methods for predicting *in vivo* pharmacokinetics using data from in vitro assays. Curr Drug Metab 2008; 9: 940–51.
Ito K, Iwatsubo T, Kanamitsu S, Nakajima Y, Sugiyama Y. Quantitative prediction of *in vivo* drug clearance and drug interactions from *in vitro* data on metabolism, together with binding and transport. Annu Rev Pharmacol Toxicol 1998; 38: 461–99.
Jonas MC, Pehar M, Puglielli L. AT-1 is the ER membrane acetyl-CoA transporter and is essential for cell viability. J Cell Sci 2010; 123: 3378–88.
Kikuchi H, Almer G, Yamashita S, Guegan C, Nagai M, Xu Z, et al. Spinal cord endoplasmic reticulum stress associated with a microsomal accumulation of mutant superoxide dismutase-1 in an ALS model. Proc Natl Acad Sci USA 2006; 103: 6025–30.
Klionsky DJ. Neurodegeneration: good riddance to bad rubbish. Nature 2006; 441: 819–20.
Ko MH, Puglielli L. The sterol carrier protein SCP-x/pro-SCP-2 gene has transcriptional activity and regulates the Alzheimer disease gamma-secretase. J Biol Chem 2007; 282: 19742–52.
Ko MH, Puglielli L. Two Endoplasmic Reticulum (ER)/ER golgi intermediate compartment-based lysine acetyltransferases post-translationally regulate BACE1 levels. J Biol Chem 2009; 284: 2482–92.
Komatsu M, Waguri S, Chiba T, Murata S, Iwata J, Tanida I, et al. Loss of autophagy in the central nervous system causes neurodegeneration in mice. Nature 2006; 441: 880–4.
Komatsu M, Wang QJ, Holstein GR, Friedrich VL, Jr., Iwata J, Kominami E, et al. Essential role for autophagy protein Atg7 in the maintenance of axonal homeostasis and the prevention of axonal degeneration. Proc Natl Acad Sci USA 2007; 104: 14489–94.
Lalonde R, Fukuchi K, Strazielle C. Neurologic and motor dysfunctions in APP transgenic mice. Rev Neurosci 2012; 23: 363–79.
Lee IH, Cao L, Mostoslavsky R, Lombard DB, Liu J, Bruns NE, et al. A role for the NAD-dependent deacetylase Sirt1 in the regulation of autophagy. Proc Natl Acad Sci USA 2008; 105: 3374–9.
Lee IH, Finkel T. Regulation of autophagy by the p300 acetyltransferase. J Biol Chem 2009; 284: 6322–8.
Lee JA. Autophagy in neurodegeneration: two sides of the same coin. BMB Rep 2009; 42: 324–30.
Leitman J, Ulrich Hartl F, Lederkremer GZ. Soluble forms of polyQ-expanded huntingtin rather than large aggregates cause endoplasmic reticulum stress. Nature Commun 2013; 4: 2753.
Lesne S, Koh MT, Kotilinek L, Kayed R, Glabe CG, Yang A, et al. A specific amyloid-beta protein assembly in the brain impairs memory. Nature 2006; 440: 352–7.
Levine B, Packer M, Codogno P. Development of autophagy inducers in clinical medicine. J Clin Invest 2015; 125: 14–24.
Madeo F, Eisenberg T, Kroemer G. Autophagy for the avoidance of neurodegeneration. Genes Dev 2009; 23: 2253–9.
Madeo F, Tavernarakis N, Kroemer G. Can autophagy promote longevity? Nat Cell Biol 2010; 12: 842–6.
Madeo F, Zimmermann A, Maiuri MC, Kroemer G. Essential role for autophagy in life span extension. J Clin Invest 2015; 125: 85–93.
Mak AB, Pehar M, Nixon AM, Williams RA, Uetrecht AC, Puglielli L, et al. Post-Translational regulation of CD133 by ATase1/ATase2-mediated lysine acetylation. J Mol Biol 2014; 426: 2175–82.
Mangiarini L, Sathasivam K, Seller M, Cozens B, Harper A, Hetherington C, et al. Exon 1 of the HD gene with an expanded CAG repeat is sufficient to cause a progressive neurological phenotype in transgenic mice. Cell 1996; 87: 493–506.
Marino G, Madeo F, Kroemer G. Autophagy for tissue homeostasis and neuroprotection. Curr Opin Cell Biol 2011; 23: 198–206.
Marino G, Pietrocola F, Eisenberg T, Kong Y, Malik SA, Andryushkova A, et al. Regulation of autophagy by cytosolic acetyl-coenzyme A. Mol Cell 2014; 53: 710–25.
Mizushima N, Levine B, Cuervo AM, Klionsky DJ. Autophagy fights disease through cellular self-digestion. Nature 2008; 451: 1069–75.
Mizushima N, Yoshimori T, Levine B. Methods in mammalian autophagy research. Cell 2010; 140: 313–26.
Nassif M, Valenzuela V, Rojas-Rivera D, Vidal R, Matus S, Castillo K, et al. Pathogenic role of BECN1/Beclin 1 in the development of amyotrophic lateral sclerosis. Autophagy 2014; 10: 1256–71.
Nilsson P, Loganathan K, Sekiguchi M, Matsuba Y, Hui K, Tsubuki S, et al. Abeta secretion and plaque formation depend on autophagy. Cell Reports 2013; 5: 61–9.
Nilsson P, Sekiguchi M, Akagi T, Izumi S, Komori T, Hui K, et al. Autophagy-related protein 7 deficiency in amyloid beta (Abeta) precursor protein transgenic mice decreases Abeta in the multivesicular bodies and induces Abeta accumulation in the Golgi. Am J Pathol 2015; 185: 305–13.
Nixon RA. The role of autophagy in neurodegenerative disease. Nat Med 2013; 19: 983–97.
Ogata M, Hino S, Saito A, Morikawa K, Kondo S, Kanemoto S, et al. Autophagy is activated for cell survival after endoplasmic reticulum stress. Mol Cell Biol 2006; 26: 9220–31.
Ohashi Y, Munro S. Membrane delivery to the yeast autophagosome from the Golgi-endosomal system. Mol Biol Cell 2010; 21: 3998–4008.
Pehar M, Lehnus M, Karst A, Puglielli L. Proteomic assessment shows that many endoplasmic reticulum (ER)-resident proteins are targeted by Nε-lysine acetylation in the lumen of the organelle and predicts broad biological impact. J Biol Chem 2012a; 287: 22436–40.
Pehar M, Jonas MC, Hare TM, Puglielli L. SLC33A1/AT-1 protein regulates the induction of autophagy downstream of IRE1/XBP1 pathway. J Biol Chem 2012b; 287: 29921–30.
Pehar M, O'Riordan KJ, Burns-Cusato M, Andrzejewski ME, del Alcazar CG, Burger C, et al. Altered longevity-assurance activity of p53:p44 in the mouse causes memory loss, neurodegeneration and premature death. Aging Cell 2010; 9: 174–90.
Pehar M, Puglielli L. Lysine acetylation in the lumen of the ER: a novel and essential function under the control of the UPR. Biochim Biophys Acta 2013; 1833, 686–97.
Peng Y, Li M, Clarkson BD, Pehar M, Lao PJ, Hillmer AT, et al. Deficient import of acetyl-CoA into the ER lumen causes neurodegeneration and propensity to infections, inflammation, and cancer. J Neurosci 2014; 34: 6772–89.
Pickford F, Masliah E, Britschgi M, Lucin K, Narasimhan R, Jaeger PA, et al. The autophagy-related protein beclin 1 shows reduced expression in early Alzheimer disease and regulates amyloid beta accumulation in mice. J Clin Invest 2008; 118: 2190–9.
Polymeropoulos MH, Lavedan C, Leroy E, Ide SE, Dehejia A, Dutra A, et al. Mutation in the alpha-synuclein gene identified in families with Parkinson's disease. Science 1997; 276: 2045–7.
Puri C, Renna M, Bento CF, Moreau K, Rubinsztein DC. Diverse autophagosome membrane sources coalesce in recycling endosomes. Cell 2013; 154: 1285–99.
Sha H, He Y, Chen H, Wang C, Zenno A, Shi H, et al. The IRE1alpha-XBP1 pathway of the unfolded protein response is required for adipogenesis. Cell Metab 2009; 9: 556–64.
Singh SS. Preclinical pharmacokinetics: an approach towards safer and efficacious drugs. Curr Drug Metab 2006; 7: 165–82.
Takami M, Nagashima Y, Sano Y, Ishihara S, Morishima-Kawashima M, Funamoto S, et al. gamma-Secretase: successive tripeptide and

tetrapeptide release from the transmembrane domain of beta-carboxyl terminal fragment. J Neurosci 2009; 29, 13042–52.
Tamura H, Shibata M, Koike M, Sasaki M, Uchiyama Y. Atg9A protein, an autophagy-related membrane protein, is localized in the neurons of mouse brains. J Histochem Cytochem 2010; 58: 443–53.
Trombetta ES, Parodi AJ. Quality control and protein folding in the secretory pathway. Annu Rev Cell Dev Biol 2003; 19: 649–76.
Urushitani M, Ezzi SA, Matsuo A, Tooyama I, Julien JP. The endoplasmic reticulum-Golgi pathway is a target for translocation and aggregation of mutant superoxide dismutase linked to ALS. FASEB J 2008; 22: 2476–87.
van Dellen A, Blakemore C, Deacon R, York D, Hannan AJ. Delaying the onset of Huntington's in mice. Nature 2000; 404: 721–2.
Vidal RL, Matus S, Bargsted L, Hetz C. Targeting autophagy in neurodegenerative diseases. Trends Pharmacol Sci 2014; 35: 583–91.
Vidal RL, Figueroa A, Court FA, Thielen P, Molina C, Wirth C, et al. Targeting the UPR transcription factor XBP1 protects against Huntington's disease through the regulation of FoxO1 and autophagy. Hum Mol Genet 2012; 21: 2245–62.
Wang DS, Dickson DW, Malter JS. beta-Amyloid degradation and Alzheimer's disease. J Biomed Biotechnol 2006; 2006: 58406.
Wang J, Slunt H, Gonzales V, Fromholt D, Coonfield M, Copeland NG, et al. Copper-binding-site-null SOD1 causes ALS in transgenic mice: aggregates of non-native SOD1 delineate a common feature. Hum Mol Genet 2003; 12: 2753–64.
Wang Y, Shen J, Arenzana N, Tirasophon W, Kaufman RJ, Prywes R. Activation of ATF6 and an ATF6 DNA binding site by the endoplasmic reticulum stress response. J Biol Chem 2000; 275: 27013–20.
Wickner W, Schekman R. Protein translocation across biological membranes. Science 2005; 310: 1452–6.
Young AR, Chan EY, Hu XW, Kochl R, Crawshaw SG, High S, et al. Starvation and ULK1-dependent cycling of mammalian Atg9 between the TGN and endosomes. J Cell Sci 2006; 119: 3888–900.
Zhang X, Li L, Chen S, Yang D, Wang Y, Zhang X, et al. Rapamycin treatment augments motor neuron degeneration in SOD1(G93A) mouse model of amyotrophic lateral sclerosis. Autophagy 2011; 7: 412–25.